E212: Properties of Elementary Particles

Bence Mitlasóczki*and Benoît Scholtes†
Rheinische-Friedrich-Wilhelms Universität Bonn

April 3, 2018

Abstract goes here

1 Introduction

Introduction text Give details of bubble chamber, i.e. energy, year, etc

2 Theory

Our current best understanding of particle physics is the Standard Model of particle physics (SM). This model describes our discoveries of fundamental particles and their interactions with each other, mediated by fundamental forces. It furthermore describes the way these particles and forces combine to form atoms, from which many of the physical phenomena we encounter in everyday life can be explained. The main shortcoming of the SM however, is its inability to be united with gravity. That said, due to the relative weakness of gravity in comparison to the other fundamental forces, it rarely has an effect in particle physics and thus is mainly ignored.

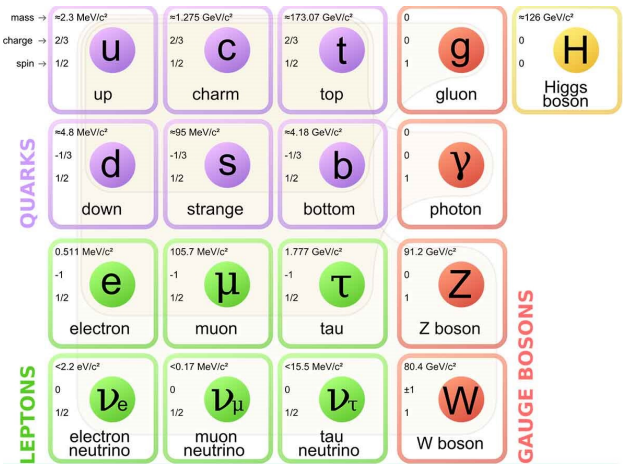

Figure 1: Illustration of the elementary particles in the SM. Quarks are in purple and Leptons in green, arranged into generation columns from left to right. The gauge bosons are in red, with the scalar Higgs boson in yellow.[5]

2.1 The Standard Model

Figure 1 give a summary of the particles in the SM with their most basic properties. Furthermore, there also exists anti-particles of many of these particles. An anti-particle, such as a positron, is identical to its particle (electron) apart from having the opposite electric charge. A neutral particle is often its own anti-particle such as the Z boson, though neutrinos have anti-particles which are merely distinct by having opposing spin projections. All matter particles and the W bosons have anti-particles while the rest are their own anti-particles. Quarks and leptons make up all the matter particles that have been discovered. These are given in three generations of particles, shown with the columns from left to right in the figure. Matter that is encountered everyday is largely structured from the first generation, namely the electron, electron neutrino, up quark, and down quark. For example, atoms are made up of electrons, protons, and neutrons, the latter two being composed of up and down quarks. The second and third generations are composed of particles which are otherwise exactly identical to their first generation counterpart apart from being heavier, the third generation being the heaviest of them all. This is only known to be true for the charged leptons (electron, muon, and tau) and quarks however. Though the neutrinos are known not to be massless, they have very small masses which have not been accurately measured. It is unknown which is the most massive and which the least.[1] Figure 2 illustrates the relative masses of the matter particles. The main reason why the second and third generation of particles are largely not existent in everyday phenomena is due to the requirement that higher energies are needed to produce these heavier particles. Furthermore, these heavier particles have shorter lifetimes due to their favourable decay into lighter particles, such as those in the first generation, due to the fundamental tendency of physical systems to higher kinetic energy states. Particle physics experiments need to be performed at increasingly higher energies in order to produce more massive particles that we do not readily observe. This is illustrated in Figure 3. It should

*s6bemitl@uni-bonn.de
†s6bescho@uni-bonn.de

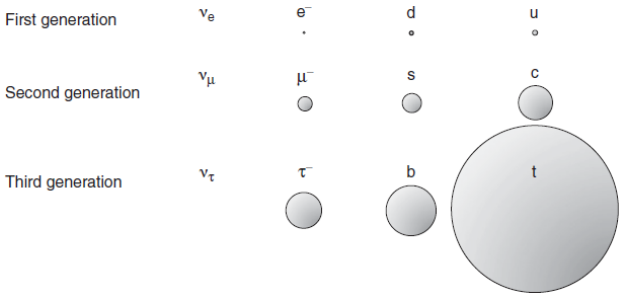

Figure 2: Illustration of the relative masses of the matter particles in their respective generations. The neutrinos are left blank to show that their masses are extremely small in comparison the other particles.[1]

be noted that though neutrinos are not seen, trillions of solar neutrinos pass through your body each second, oscillating between their three different flavours.[1] They are extremely difficult to detect due to the fact that they have a small mass and no electric charge.

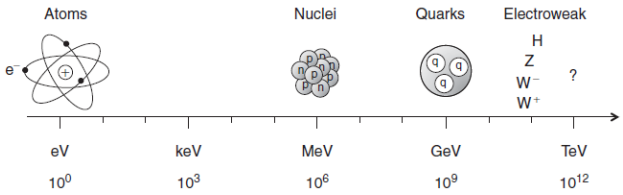

Figure 3: Illustration of the energies required to probe different structures and particles.[1]

Figure 1 also shows the fundamental forces in the SM which are all mediated via the exchange of a gauge boson. The most familiar of these is the photon γ which mediates the electromagnetic force, responsible for electricity, magnetism, and light. The photon interacts with all particles that have an electric charge and thus with all matter particles in the SM apart from the neutrinos. It also interacts with the W bosons as they are electrically charged. The gluon gauge bosons mediate the strong force, thus called as it is the strongest force and binds nuclei and hadrons together, explained in Section **??**. The gluons interacts only with particles which have a so-called "colour" charge, another property of particles similar to electric charge. Only quarks have a colour charge and the eight differently coloured gluons. Next, the oppositely charged $W^{\pm}$ and Z bosons mediate the weak interaction, the weakest force apart from gravity. This force is responsible for radioactive decay and interacts with all matter particles in the SM. Finally, the Higgs boson is the most recently discovered particle which gives mass to all the matter particles in the SM by interacting with them.

2.2 Hadrons and the Strong Force

Though quarks are elementary in the SM, they cannot be observed as free particles. This is because quantum chromodynamics (QCD) of the SM, the theory of the strong force, states that colour is confined such that systems with a colour charge cannot propagate freely, termed *colour confinement*. Instead, only colourless composite particles can be observed. As a result, quarks form composite particles called hadrons which are bound by gluons. Hadrons generally form baryons, composed of three quarks, and mesons, composed of one quark and one anti-quark. The reason for the these two types is a result of there being three colours, red, blue, and green, for the quarks, and three anti-colours, anti-red, anti-blue, and anti-green, for the anti-quarks. Colourlessness is achieved by combining all three colours (or anti-colours) in a baryon, or a colour and its anti-colour in a meson, as shown in Figure 4. Protons and neutrons are examples of baryons, composed of two up quarks and one down quark (written as uud), and two down quarks and one up quark (udd), respectively. Furthermore, exotic hadrons, which

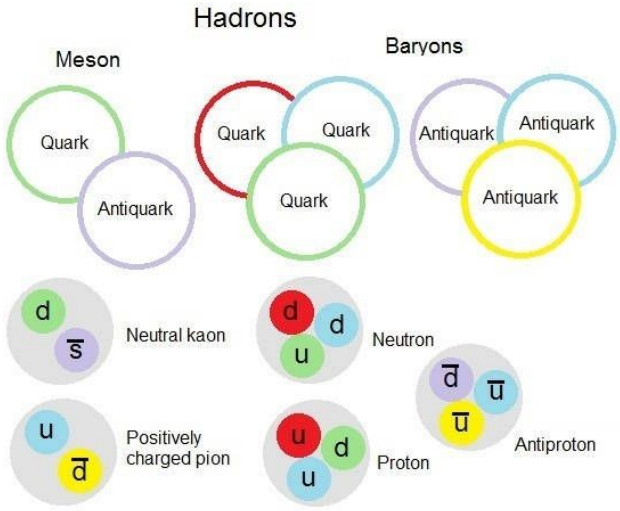

Figure 4: Colour confinement resulting in baryons and mesons, given with some examples.[6]

achieve colour confinement with more quarks, have been hypothesised and observed, though without explicit confirmation that the observations were indeed bound exotic hadrons. Examples include the tetraquark with two quarks and two respective anti-quarks, and the pentaquark with four quarks and an anti-quark. Exotic hadrons are rare however, due to the tendency of quarks to form and decay quickly into mesons and baryons.

2.3 Multiplets

The quark model of QCD just explained was originally proposed from a group theoretic perspective by Murray Gell-Mann among others in the 1960s. This method has

proven to be extremely accurate at predicting particles and their properties, explaining all the hadrons that have been observed. It predicts all the possibilities of obtaining colourless composite particles from the quarks in the SM, as well as the colours and the anti-colours. Hadrons are often grouped into so called "multiplets" in this framework by their composite particles. Figure 5 shows one such multiplet of mesons formed from up, down, and strange quarks, as well as their anti-quarks. Noteworthy

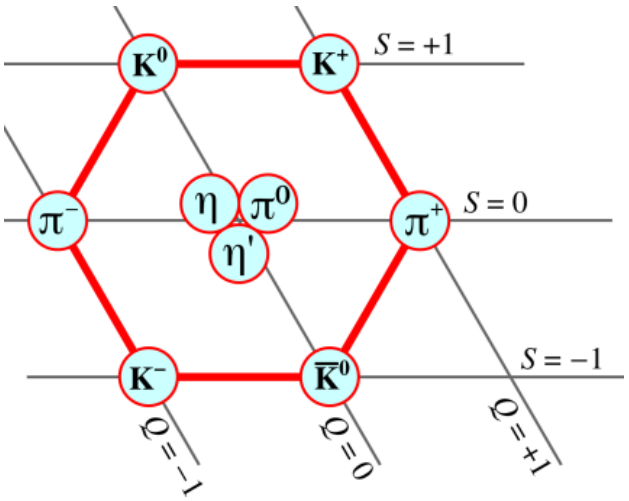

Figure 5: The light pseudoscalar meson nonet, plotted against strangeness and electric charge axes.[7] It is called the light nonet as it is composed of the lightest quarks, resulting in the lightest meson multiplet.

is the strangeness quantum number, shown in the figure, defined as $S = n_{\bar{s}} - n_s$, where $n_{\bar{s}}$ and n_s are the number of strange anti-quarks and quarks in the hadron, respectively.[1] Strangeness has been observed to be conserved in strong and electromagnetic interactions, but not in weak interactions. The pions and neutral kaon are of particular importance of this experiment. The $\pi^{\pm}$, π^0, and K^0 have masses[8]

$$\begin{aligned} m_{\pi^{\pm}} &= (139.57018 \pm 0.00035)\ \text{MeV}, \\ m_{\pi^0} &= (134.9766 \pm 0.0006)\ \text{MeV}, \\ m_{K^0} &= (497.61 \pm 0.013)\ \text{MeV}. \end{aligned}$$

The main decay modes of the pions are

$$\begin{aligned} \pi^+ &\to \mu^+ \nu_\mu \to (e^+ \nu_e \overline{\nu}_\mu)\, \nu_\mu, \\ \pi^- &\to \mu^- \overline{\nu}_\mu \to (e^- \nu_\mu \overline{\nu}_e)\, \overline{\nu}_\mu, \\ \pi^0 &\to 2\gamma, \end{aligned}$$

where the resulting decays of the muons are given in brackets. The branching ratios of these pion decays are 99.99% for the charged pions and 98.82% for the neutral pion, showing that these particular decays largely dominate pion decays.[8] In this experiment however, the π^- has a much higher probability of participating in a scattering process $\pi^- + p \to \pi^0 + n$ due to the proton-rich liquid hydrogen and thus any so-called $\pi\mu e$ decay observed will most likely be a π^+ decay. It should be noted that there exists other meson multiplets apart from the one shown in Figure 5, composed of other quarks.

Figures 6 and 7 show two examples of baryon multiplets that are relevant in this paper. Both the octet and

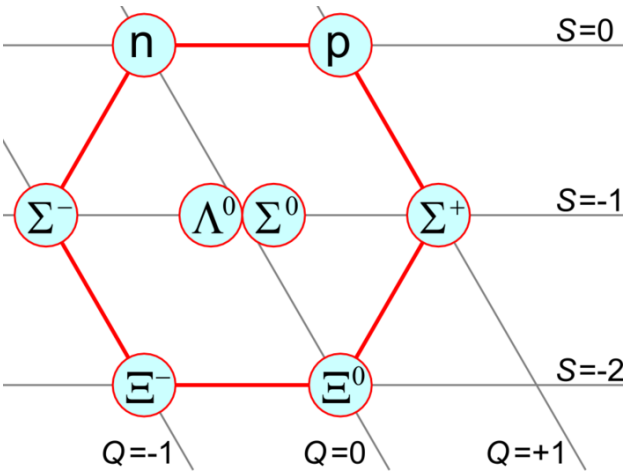

Figure 6: The light baryon octet.[9] Note the similarity to the mesons nonet, yet composed of one less particle and having no positive strangeness particles as none are composed of anti-strange quarks.

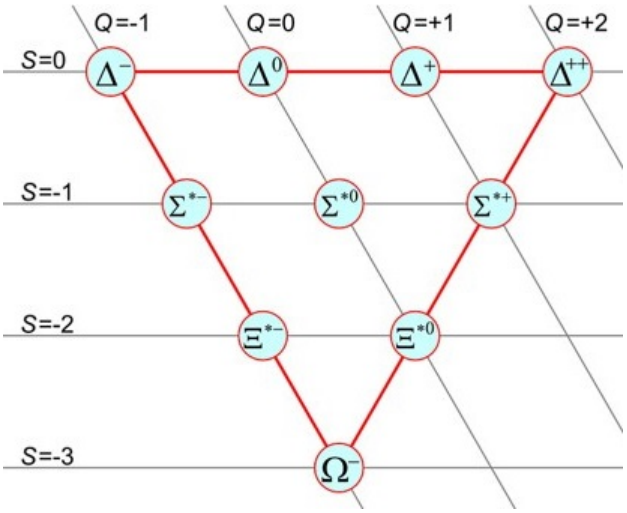

Figure 7: The light baryon decuplet.[10]

decuplet are composed of baryons containing up, down, and strange quarks. It is interesting to note that many of these particles are composed of the same quarks, such as the proton and Δ^+, both composed of two up quarks and a down quarks. The difference is the linear combination of these quarks, accounting for the different ways

that the quarks can be "arranged" in the baryon. As such, the quark wavefunction of the two particles are[1]

$$p = \frac{1}{\sqrt{6}}(2uud - udu - duu)$$
$$\Delta^+ = \frac{1}{\sqrt{3}}(uud + udu + duu)$$

Thus, while the proton has a mass $m_p = (938.2720813 \pm 0.0000058)$ MeV and spin of $J_p = 1/2$, the Δ baryons have a mass of $m_\Delta = (1232 \pm 2)$ MeV and spin of $J_\Delta = 3/2$.[8] As a result, the Δ^+ baryon is called a higher-mass excitation of the proton. Though the proton is stable, being the only stable baryon, Δ^+ has a mean lifetime of $\tau_{\Delta^+} = (5.63 \pm 0.14) \times 10^{-24}$ s with primary decays $\Delta^+ \to \pi^0 + p$ or $\pi^+ + n$, though the branching ratios are not yet known.[8] The difference in linear combination of composing quarks is also the reason why the three mesons grouped in Figure 5 with $S = Q = 0$, the neutral pion, and the η and η' prime mesons, are all different particles yet made up of the same quarks.

2.4 Kinematics

In order to discover and identify new particles, particle physics experiments primarily analyse the kinematics of particle interactions. This allows for a calculation of the particle's mass, while the other particles involved in the interaction mean that the properties of the particle, such as electric charge and spin, can be determined. The universally fulfilled conservations of energy and momentum in a closed system are largely employed to calculate the mass of unknown particles. To do so, the masses and velocities of the other particles involved in the interaction need to be measured which is easily achieved by analysing bubble chamber photographs.

2.5 The Bubble Chamber

A bubble chamber is used in certain particle physics experiments to photograph collisions such that the involved particles can be tracked. From this, the particles can be identified and their energies and momenta can be calculated. New particles can thus be discovered who don't match the description of known particles. A bubble chamber is simply a large container filled with transparent liquid, in this experiment liquid nitrogen, held at a temperature just below boiling point.[4] A piston then causes a fast expansion of the liquid, causing the liquid's boiling point to suddenly drop below then temperature of the liquid. This causes the liquid to be in a metastable state, whereby it does not boil unless stimulated by disturbances. Such disturbances can be imperfections of the container's surface or the ionisation of atoms in the liquid. This is exploited by bubble chamber experiments as charged particles travelling through the liquid will cause the ionisation of surrounding atoms as a result of Bremsstrahlung, thereby leaving ionisation tracks formed of microscopic bubbles of vapour. These are then allowed to grow in size to $0.01-0.1$ mm until they can be visibly photographed, such that the tracks of the charged particles can be seen. A uniform magnetic field is also passed through the liquid such that the charges and velocities of the particles can be determined from the directions of deflection and radii of track arcs. To reconstruct a 3D visualisation of the interactions, multiple cameras arranged at different angles are used. In this experiment, only track which lie approximately in the same plane (with an inclination angle of <18%) are analysed, meaning that spatial reconstruction will not be necessary. Photographs from different angles will be used to clarify interactions however. Figure 8 provides a diagram of the process.

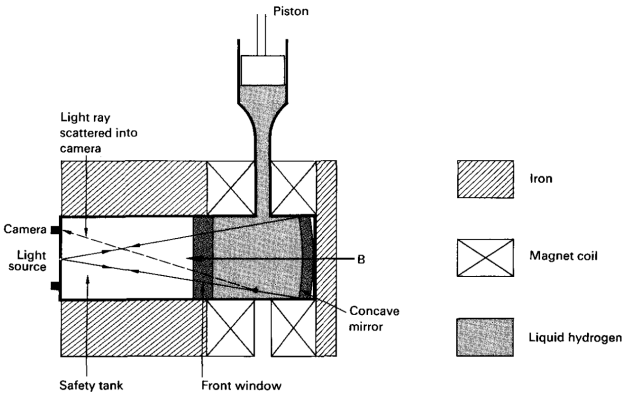

Figure 8: Cross section of a bubble chamber. The particle beam travels normal to the paper.[11]

3 Procedure

This experiment only analyses photographs taken at the proton-synchrotron at CERN in 1971. No bubble chamber experiments were conducted. Several hundred photographs from three different cameras are projected onto a measuring table and can be superimposed and moved. Measurements can be made on the table to determine the properties of the observed particles. This section summarises the method used.

3.1 Magnification

Figure 9 shows an example of a bubble chamber photograph. To be able to start analysis on such photographs, their magnifications need to be determined so that calculations of track radii can be accurately calculated. The magnification of the photographs are affected by the distance away the tracks are from the camera, as well as the depths and refractive indices of the liquid hydrogen and container glass that the light must pass through before

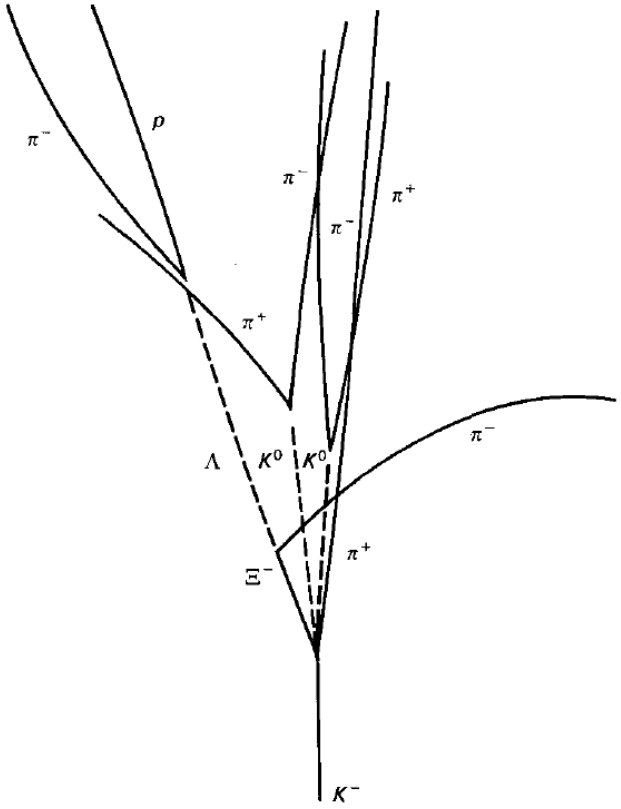

Figure 9: Example of a $\Sigma^- \to \pi^- + \Lambda$ decay in a bubble chamber, whereby the particle tracks have been obtained from a photograph. The solid lines depict the ionisation tracks of charged particles while the dotted lines are extrapolated tracks of neutral particles, which do no produce ionisation tracks nor are they deflected by the magnetic field.[11]

reaching the camera. The magnification scale is determined using markers on the front and back windows containers which have known separation lengths. As a result, by measuring their separations on a photography, the magnification of the photograph V_A can be determined using[4]

$$V_A = \frac{V_F + V_G}{2}, \tag{1}$$

Here, V_F and V_G are the magnifications of the front and back markers respectively, where $V_F = \Delta f / \Delta f'$ (and similarly for V_G) is the ratio between the marker separations on the photograph and on the glass pane, respectively. In the derivation of Equation 1, it was assumed that the particle beams travelled in the middle of the chamber, halfway between the front and back glass, as the true depth is unknown. That said, as the particle beam is always approximately incident in the middle of the bubble chamber and the always take pictures with the same zoom, the same magnification can be used for all photographs. The inclination angle range of 18% introduces error into this method however, as the calculated magnification is indeed not completely accurate for all particle tracks.

3.2 Charge Sign

Once the magnification of the photographs is known, the direction of the magnetic field must be determined so that the charge sign of particles can be determined. This is achieved simply by observing the deflection of *δ-electrons*, as seen in Figure 10. These are electrons

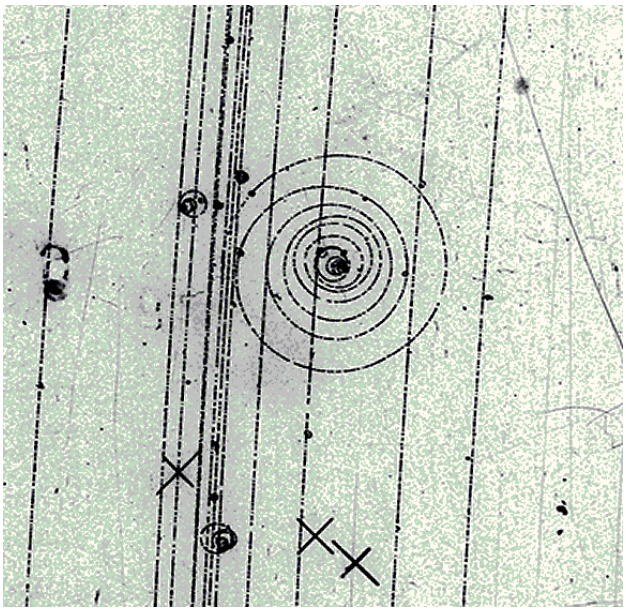

Figure 10: Example of a δ-electron spiral, showing the deflection of negatively charged particles. The straight lines are ionisation tracks while the crosses near the bottom are markers on the glass.[12]

which are ejected from their atoms by closely passing charged particles. These leave behind small spirals originating from ionisation tracks. The direction of the spirals then indicate the direction that negatively charged particles deflect. These are spirals instead of circles as their constant bremsstrahlung emissions causes them to lose energy and thus velocity. This causes them to travel in increasingly smaller circles as a result of the Lorentz force in the same magnetic field strength.

3.3 Momentum Calculations

The momenta can now be calculated by determining the radii r' of the tracks in the photographs, and using the magnification V and the magnetic field strength B. The radii r' can be determined using stencils which display arcs of different radii to be matched with the arc in question. The momentum of a particle is then

$$p = 0.3 \cdot B \cdot V \cdot r', \tag{2}$$

derived by equating the centrifugal force on the particle apparent from the curvature of the track and the Lorentz

force from the magnetic field which causes this curvature.[4] Due to the decreasing radii of the track spirals, the first section of the spiral is to be used with the stencils to estimate the initial momentum of the particle after a vertex. That said, a large enough section of the spiral should be used to more accurately determine the radii and thus momentum. Uncertainty was estimated by the confidence in accuracy of a calculated radius. This method will be used to calculate the momentum of observed particles such that the mass of

3.4 Stereo-shift Method

The *stereo-shift method* uses two cameras to determine the depth of ionisation tracks in the bubble chamber. This will be herein used to determine the accuracy of the assumption that the particle beams travelled through the centre of the chamber, used in Section 3.1. In the method, photographs from two cameras of the same event are superimposed such that the same marker on the front glass are on top of one another. The distances between a marker on the back glass and between a point on or close to an ionisation track in both photographs are then measured. This then allows for a calculation of the depth of said track a_z, using the following equation:[4]

$$a_z = \frac{g_z s_A}{s_G}, \tag{3}$$

where g_z is the depth of the chamber, and s_A and s_G are the measured distances between the points on the ionisation track and the back glass markers, respectively, as shown in Figure 11. The branching of a δ-electron

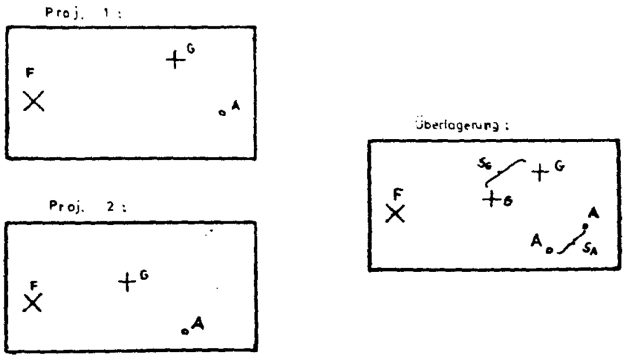

Figure 11: Demonstration of the stereo-shift method, with the two photographs used from different cameras shown on the left and the superimposed image on the right, with the distances shown.[4]

spiral from a track as seen in Figure 10 was often used as a point A in a photograph to determine the depth as they are easy to spot and are located on an ionisation track.

3.5 Proton-proton Cross-section

The cross-section of a particle interaction is the area perpendicular their relative motion in which the two particles must cross in order to scatter.[1] The probability that two particles will scatter is proportional to their cross-section and thus scattering probabilities are often quantified as such. The proton-proton cross-section can be calculated by observing the difference between the number of incident protons into the chamber and those leaving, averaging over a large number of beam runs. The average difference then equals the average number of proton-proton collisions, from which the cross-section σ can be calculated. The number of protons passing through the bubble chamber (in the x-direction) obeys[4]

$$N(x) = N_0 e^{-n\sigma x} \tag{4}$$

with N_0 being the number of protons incident to the chamber and n is the number density of scatterings per unit volume, given by

$$n = \frac{\rho N_A}{A} = 3.79 \times 10^{22} \text{ cm}^{-3},$$

where $\rho = 0.126$ g cm^{-3} is the density of liquid nitrogen, N_A is Avogadro's constant, and $A = 2$ g mol^{-1} is the composition of the liquid nitrogen used in the bubble chamber.[13] Equation 4 will be used to calculate the total and inelastic cross-sections of the proton-proton interactions.

3.6 π^0 Multiplicity

One can calculate the average number of neutral pions produced in proton-proton collisions by directly observing how many were produced in the total number of proton-proton collisions considered. Since the neutral π^0 is invisible in the bubble chamber photographs however, the number of π^0 produced must instead be calculated by observing the number of $\gamma - \gamma$ productions from the $\pi^0 \to \gamma\gamma$ decay. The photons are again invisible in the chamber however, and thus their multiplicity must be determined from the number of $\gamma \to e^- + e^+$ pair productions observed. The probability that a photon decays to an electron-positron pair at a distance d away from its production is[4]

$$P(d) = \frac{1}{\lambda_{abs}} e^{-d/\lambda_{abs}},$$

where $\lambda_{abs} = 1146$ cm is the absorption length of a photon in liquid hydrogen. That said, the photographs only determine whether a pair production has been produced in the bubble chamber only, not accounting for decays after leaving the chamber. The probability that a photon decays within the chamber of length L_c m is then

$$P_c = 1 - \lambda_{abs}/L_c + (\lambda_{abs}/L_c)e^{-L_c/\lambda_{abs}} = 0.08240, \tag{5}$$

which takes into account that not all photons will be produced at the same point along the length of the chamber.[4] The total number of neutral pions created can then be calculated using

$$m_{\pi^0} = \frac{n_{\text{pp}} \cdot L_c}{2 \cdot n_{\text{inel}} \cdot \left((\lambda_{abs} \cdot e^{-L_c/\lambda_{abs}} - 1) + L_c \right)}, \qquad (6)$$

where n_{pp} and n_{inel} are the observed number of pair productions and inelastic collisions.[4] Thus, by counting the number of pair productions seen for the total amount of proton-proton collisions, the π^0 multiplicity can be calculated. The multiplicity can also be calculated from the average charged multiplicity of proton-proton collisions, being the average number of charged particles produced in such a collision. Since there are on average four charge particles created per neutral pions in high-energy proton-proton collisions, the average neutral pion multiplicity can be estimated by dividing the calculated charge multiplicity by four.[14] This allows us to compare the results of the two calculations to determine their accuracy.

4 Results

4.1 Magnification and Beam Depth

The magnification was firstly calculated from a single photograph using the method described in Section 3.1. The F21, F22 and G41, G42 markers on the front glass and back glass, respectively, were used. These have an actual separation of $l_F = 23.9951$ cm and $l_G = 32.1905$ cm, though we measured their separation on the photograph at (28.2 ± 0.1) cm and (37.7 ± 0.1) cm, respectively. Using Equation 1 we obtained a magnification of $V_A = 0.852 \pm 0.003$, which is used when analysing all photographs in this paper.

To get the true depth at which the beams were passing through, we used the *stereo-shift method* in 23 different cases. Viewing the same event from two different cameras, we measured the displacement s_G of the G41 marker and s_A of an easily identifiable event in the path of the beam, both with measurement uncertainties of ± 0.1 cm. The distribution of the measured s_A values are shown in Figure 12. We can see that the measurements approximately follow a Gaussian distribution though only roughly due to the small sample value. This however demonstrates the distribution in beam depths in different photographs, introducing error from a single depth used to calculate the magnification. From the data gathered and Equation 3, we discovered the depth to be at

$$\frac{s_A}{s_B} = 0.570 \pm 0.021,$$

of the total depth, which is in disagreement with our assumption made to calculate the magnification, namely that the beam passes through at 0.5 depth. This is an important source of systematic error when converting measured lengths and radii on to the photographs to real values.

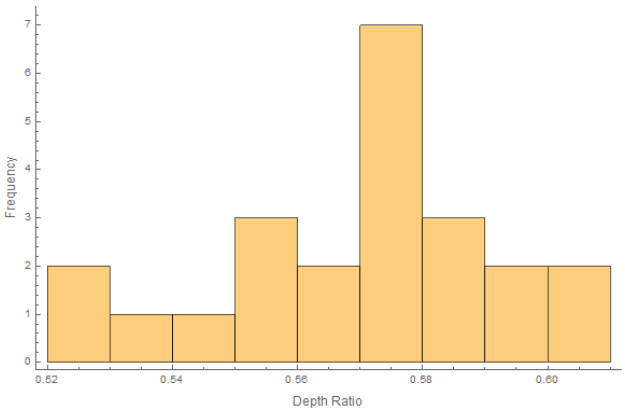

Figure 12: Plot of the measured s_A/s_B values used for the stereo-shift method.

4.2 Proton-proton Cross-section

Next 50 photographs were analysed by identifying and counting elastic and inelastic scatterings between the marks F21 and F35 of the front glass. These marks were used as they nearly span the whole length of the chamber and the distance between them could be easily measured with little uncertainty. The length was measured at (174.5 ± 0.1) cm, which gives an unmagnified distance of $L = (148.739 \pm 0.085)$ cm. Of the 532 total incoming protons, 27 of them interacted with the hydrogen in the chamber via elastic scattering while 64 scattered inelastically, accounting to 91 total scatterings. Since only 50 photographs were analysed however, we can estimate the error in the scattering values as originating from binomial error due to the polarity of the outcomes being scattering or no-scattering, and elastic scattering or no scattering.[3] Thus, for the total cross section we obtained $N_{\text{t}}(L) = 91 \pm 9$, and $N_{\text{e}}(L) = 27 \pm 5$ for the elastic cross section. These values yield

$$\sigma_{\text{elastic}} = (9.3 \pm 1.8) \text{ mb},$$
$$\sigma_{\text{total}} = (33.4 \pm 3.5) \text{ mb}.$$

These are in agreement with theoretical cross-sections of $\sigma_{\text{elastic}} = (7.9 \pm 0.1)$ and $\sigma_{\text{total}} = (38.8 \pm 0.1)$ mb,[?] though the uncertainties of the total cross-sections don't overlap. This could be caused by the inaccurately calculated magnification thus affecting the calculated length in which scatterings were counted. Otherwise, we may have observed a statistically unlikely small number of scatterings not completely accounted for by the binomial uncertainty. The calculated values nevertheless suggest agreement with what was to be expected.

4.3 Pion Multiplicities

Of the 64 inelastic scattering events, 11 had two, 35 had four, 13 had six, and 5 had eight outgoing charged particles, respectively. This gives a total of 280 charged particle tracks from 64 events, giving an average charged multiplicity of $m_{\text{chg}} = 4.375$. This matches our expectations from previous proton-proton collision experiments with 24 GeV/c incident momentum (giving a total energy of $s \approx 47$ GeV^2).[14] From this, the π^0 multiplicity can be estimated to be approximately

$$m_{\pi_0} = \frac{m_{\text{chg}}}{4} = 1.094.$$

At high energies, positive, negative and neutral pions are approximately created in equal numbers, where at our energies we expect the multiplicity to be around 1.3 ± 0.3 for each individual pion.[11,14] This provides some confidence in our multiplicity estimation above.

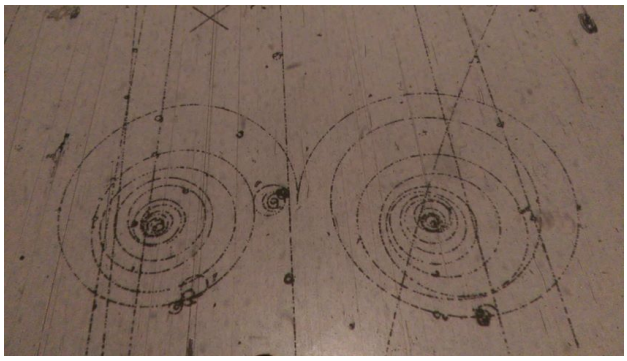

Figure 13: Example of a pair production found.

We can also calculate the neutral pion multiplicity from the detected pair productions. We found 4 such events from all the proton-proton collisions observed. Figure 13 shows one pair production found. Using Equation 6, we obtain a total neutral pion multiplicity of $m_{\pi_0} = 0.5026 \pm 0.0003$, where the uncertainty comes mainly from the uncertainty of the measured length L_c of the chamber. This result is in disagreement with the first, only being half of that value. The reason is likely due to a statistically low pair production count, given that we expect at least double from literature. Further experiments should analyse other photographs, or a large sample, to determine whether more pair productions are observed giving a higher neutral pion multiplicity.

4.4 Neutrino Momentum

A $\pi\mu e$ decay was observed, shown in Figure 14. It was found to be a $\pi^+ \rightarrow \mu^+\nu_\mu \rightarrow (e^+\nu_e\overline{\nu}_\mu)\,\nu_\mu$, decay due to the deflection of the particles showing positive charges. Using the radii stencils, we found that the pion had an initial radius of 27.0 ± 0.9 cm giving a momentum of 120.1 ± 3.8 MeV/c. The track length was measured

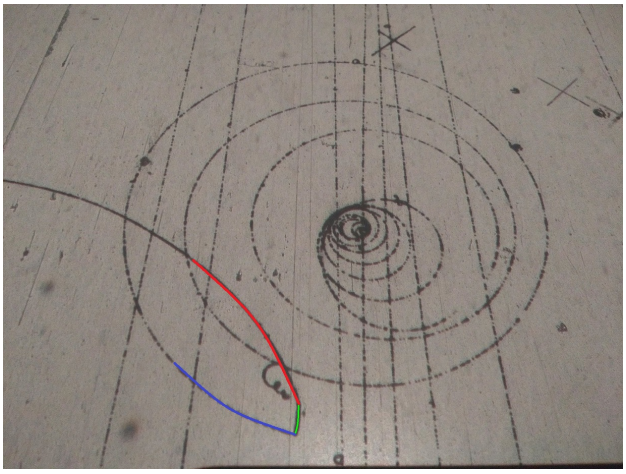

Figure 14: Image of the found $\pi\mu e$ decay, with the π^+ track coloured in red, μ^+ in green, and positron in blue. The neutrinos are all invisible in the bubble chamber as they are neutral particles.

to be 79.3 ± 0.9 cm by superimposing a piece of rope along the length of the track and then measuring the rope. A Bragg curve graph, relating the distance travelled by a charged particle and its energy loss due to its ionisation of the hydrogen, gave an initial momentum of 128.5 ± 5.9 MeV/c for this distance travelled. Seeing that these two momentum values are quite close to each other, we can infer that the pion has indeed decayed while approximately at rest in the laboratory frame. This is important as the centre-of-mass frame of the decay, in which the pion has zero momentum, is applicable. As a result of momentum conservation, the pion's decay products mu^+ and ν_μ will have equal momentum in opposing directions in this frame. The momentum's magnitude is only dependent on the mass of the pion and muon, as the neutrino mass is so small, and is easily calculated to be 29.8 MeV/c, providing us with a theoretical momentum value for the produced muon and muon-neutrino.[4] Experimentally, we measured the length of the μ^+ track to be 0.597 ± 0.085 cm. Using the Bragg curve graph again, a momentum of 27.64 ± 1.26 MeV/c was read, which is fairly good agreement with the theoretical value quoted above. This provides confidence that the identified decay is indeed a positively charged $\pi\mu e$ decay.

4.5 First Strange Particle

We analysed two neutral strange particle V^0 decays vertices in order to identify the neutral particles. To analyse them, the decays needed to be secondary vertices, in that the neutral particles were created directly from proton-proton collisions, to reduce the complexity of the method. It is important to note that the angle between the two produced particles in each case was close to 0°, so the possibility of these being pair productions

is considerable and needs to be considered. Generally, a candidate V^0 was distinguished from a pair production from the size of spirals of the decay products, expecting larger momenta and thus spirals from a heavy neutral particle decay. The first neutral particle decay was observed with a primary vertex which had two visible outgoing particles and one distant vertex of two particles with opposite charges which is suspected to have come from the primary vertex. The opposite charges of the candidate secondary vertex confirms that this is a decay of the neutral particle as the total charge is zero, while a collision with a proton would have produced a vertex of total charge +1e. The primary and candidate secondary vertices of the first neutral particle creation and decay observed are shown in Figures 15 and 16. The distance of the two vertices was measured to be (138 ± 1) cm.

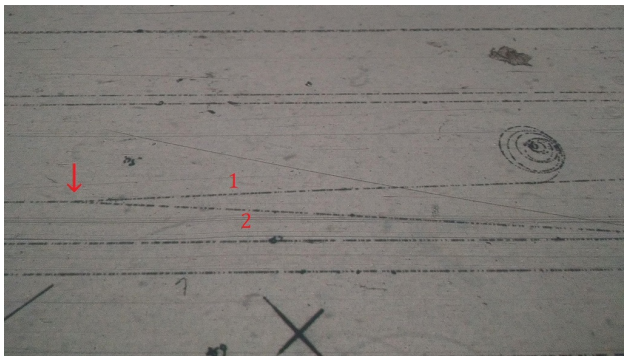

Figure 15: Image of the primary vertex (shown with the arrow) for the first neutral particle decay found, with two positively charged particles emerging from the vertex (both curved downwards), labelled for clarity.

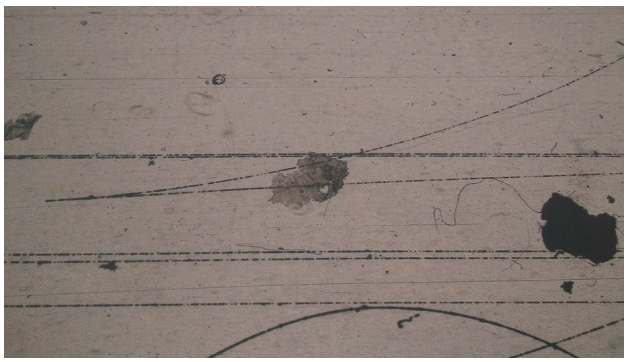

Figure 16: Image of the candidate secondary vertex for the first neutral particle decay found, seen as the tracks forming a "V" shape with no tracks to the left of it. It can be seen that the angle between the momenta of the two decay products are approximately 0°.

4.5.1 The secondary vertex

The neutral particle decayed into two particles with an angle of $(0 \pm 0.1)°$ between them. To find association with the primary vertex, we simply used a rule to see whether both particles can be directly traced back to the primary vertex, which was indeed found to be the case. We measured the two radii to be (56 ± 2) cm for the negatively charged and (750 ± 50) cm for the positively charged particle, respectively. From Equation 2, in a coordinate system with the x-axis along the supposed V^0 path, we get

$$p_- = (249.2 \pm 8.9)\,\mathrm{MeV/c},$$
$$p_+ = (3337 \pm 223)\,\mathrm{MeV/c},$$

both purely in the x-direction. The total V^0 momentum is then

$$|p_0| = (3586 \pm 223)\,\mathrm{MeV/c}.$$

4.5.2 A first look at the primary vertex

The primary vertex consists of the incoming proton, and two positively charged outgoing particles. Figure 17 is a diagram of the tracks shown for clarity. Particle 1 has

Figure 17: The first primary vertex examined, with the charged decay products given by solid lines, the V^0 by a dashed line, and the x-axis by a dotted line.

a path with radius (2000 ± 200) cm and angle $(2 \pm 0.3)°$, using the incoming proton beam as x-direction in this coordinate system, while particle 2 has a momentum of (1700 ± 100) cm and angle $(4.5 \pm 0.3)°$. The momenta of the particles are

$$p_1 = ((8893 \pm 890)\,\mathrm{MeV/c}, \quad (311 \pm 56)\,\mathrm{MeV/c}),$$
$$p_2 = ((7541 \pm 444)\,\mathrm{MeV/c}, \quad (-594 \pm 53)\,\mathrm{MeV/c}),$$
$$p_0 = ((3586 \pm 223)\,\mathrm{MeV/c}, \quad (63 \pm 19)\,\mathrm{MeV/c}),$$
$$\Sigma p = ((2.002 \pm 0.102) \cdot 10^4\,\mathrm{MeV/c}, \quad (-220 \pm 79)\,\mathrm{MeV/c}),$$

where p_0 is the momentum of the neutral strange particle and Σp is the sum of the momenta. The momenta of the three particles do not add up to the momentum of the incoming proton of 23877 MeV/c in the x-direction, where the second proton is stationary in the liquid.[4] The possibilities for this are that one or more other neutral particle were created in either vertex which were not detected as they did not decay or collide inside the chamber, or that the V^0 is not in fact a originating from the primary vertex, though it is in-line with it. It is also possible that

the V^0 is a higher vertex, whereby another neutral particle was created at the primary vertex, travelled a very short distance, then decayed into a number of neutral particles, one of whose decay was observed as the V^0. The original neutral particle would have had to travel a very short distance so that when we traced back the momenta of the V^0 decay products, the V^0 still seemed to originate from the primary vertex. These possibilities will be considered to explain the missing mass.

Name	M (MeV)	Dist. (m)	Decay	Γ_p/Γ
Λ^0	1115.7	0.079	$\mathrm{p}\,\pi^-$	63.9%
K^0_S	497.6	0.027	$\pi^+\,\pi^-$	69%
K^0_L	497.6	15.3	$\pi^\pm\,e^\mp\nu_\mathrm{e}$ $\pi^\pm\mu^\mp\nu_\mu$	40.6% 27.0%
Σ^0	1192.6	$2.22\cdot10^{-11}$	$\Lambda\,\gamma$	100%

Table 1: Possible neutral particles with masses, distances, decay products, and branching ratios of the decay products. K^0_S and K^0_L refer to the short and long-lived neutral kaon, respectively.[8]

4.5.3 Identifying the strange particle

Though there is missing momentum, it does not seem to come from the secondary vertex as the directions of the decay particles already trace back to the primary vertex, whereas another decay product would change this. The only possibility would be that a neutral particle would have a pro- or retrograde motion, though this is unlikely. Looking at Table 1, we see three possible scenarios:

- The V^0 is a Λ^0 particle, while another neutral particle left the primary vertex undetected, and the secondary vertex then contains a proton and a pion.
- The V^0 is a K^0_S particle, which decayed into a pair of pions, again with undetected neutral particles.
- A Σ^0 was created at the proton-proton collision, which then decayed very quickly, resulting in a Λ^0 baryon whose decayed into a proton, pion, and photon was observed as the incorrectly-labelled "secondary vertex".

In these scenarios, the mass of the strange particle is

$$m_{\mathrm{V}_0}(\mathrm{p},\,\pi^-) = (1103.2 \pm 1028.3)\,\mathrm{MeV},$$
$$m_{\mathrm{V}_0}(\pi^+,\,\pi^-) = (532.8 \pm 2132.2)\,\mathrm{MeV},$$

which are both within uncertainty ranges of the Λ^0 and K^0 masses. That said, the uncertainty is extremely large in both cases, though not emerging from any particular measurement. To reduce these errors, more precise experiments are required. As a result, these mass measurements have not helped us determine the identity of the neutral particle.

4.5.4 Primary vertex revisited

The missing momentum must thus come from the primary vertex, which can help us identify the strange particle. The missing momentum is

$$p_\mathrm{missing} = ((7743.0{\pm}994.5)\,\mathrm{MeV/c}, (282.9{\pm}76.9)\,\mathrm{MeV/c}).$$

It turns out that the simplest proposition for the missing momentum is the Σ^0 particle scenario. To see this, we can check the conservation laws:

- Baryon number: the Σ^0 (uds) gives 1, this means only one of the created charged particles in the primary vertex can be a baryon.
- Strangeness: Σ^0 has $S = -1$, the baryon or other particle should have an $\bar{\mathrm{s}}$ quark.
- Flavours: the baryon and the other particle should have 3 u, 1 d, and 1 $\bar{s}$ quarks.

From this, we can determine that the created baryon is a proton (uud) while the other a positively charged kaon (K^+, $\mathrm{u}\bar{\mathrm{s}}$). To check whether this is feasible, we can used energy conservation. The initial energy is $23895+938 = 24833$ MeV. If we assume that particle one is a proton, and two is the kaon, these then have energies $E(p_1,\,p^+) = (8948 \pm 884)$ MeV and $E(p_2,\,K^+) = (7580 \pm 442)$ MeV. Finally, the missing energy from the Σ^0 is $E(p_\mathrm{missing}, \Sigma^0) = (7543{\pm}981)$ MeV, giving an overall energy of $(2.407 \pm 0.140) \times 10^4$ MeV, which matches the initial energy. Switching the proton and kaon tracks yields $(2.408 \pm 0.140) \times 10^4$ MeV which is also a valid result, thus we cannot uniquely assign the two final particles to tracks. Ultimately, we explain the event as a $\mathrm{p\,p} \to \mathrm{p\,K^+}\,\Sigma^0$, $\Sigma^0 \to \gamma\,\Lambda$ collision, where we detected the $\Lambda \to \mathrm{p}\,\pi^-$ decay. Momentum and energy conservation are both well satisfied in this scenario, giving confidence in our result.

4.6 Second Strange Particle

5 Conclusion

References

[1] M. Thompson, *Modern Particle Physics* (Cambridge University Press, New York, 2013).

[2] Unspecified author, *Advanced Laboratory Course (physics601): Description of Experiments* (University of Bonn, 2018).

[3] W. R. Leo, *Techniques for Nuclear and Particle Physics Experiments* (Springer-Verlag, 1987), p. 305.

[4] G. Seul, *Properties of elementary particles* (University of Bonn, 2009).

[5] T. DeMichele, *The Standard Model (of Particle Physics) Explained*, WWW Document, http://factmyth.com/the-standard-model-of-particle-physics-explained/.

[6] H. Klus, *The Strong Nuclear Force*, WWW Document, http://www.thestargarden.co.uk/Strong-nuclear-force.html.

[7] J. Denker, *Quarks ->Mesons ->Nonet = Octet plus Singlet*, WWW Document, https://www.av8n.com/physics/quark-meson-nonet.htm.

[8] C. Patrignani et al. (Particle Data Group), Chin. Phys. C, 40, 100001 (2016) and 2017 update.

[9] Unspecified author, *Barion*, WWW Document, http://quimica.wikia.com/wiki/Bari%C3%B3n.

[10] T. Dorigo, *Omega b: the new baryon nailed by D0*, WWW Document, https://dorigo.wordpress.com/2008/09/19/omega-b-the-new-baryon-nailed-by-d0/.

[11] D. H. Perkins, *Introduction to High Energy Physics* (Addison-Wesley Publishing Company, Reading, 1972).

[12] G. T. Jones, *Pretty knock-on electron (delta-ray)*, WWW Document, http://hst-archive.web.cern.ch/archiv/HST2005/bubble_chambers/BCwebsite/gallery/gal2_12.htm.

[13] G. G. Harigel, *Bubble Chambers, Technology and Impact on High Energy Physics* (CERN, Geneva, 2003), http://web.ihep.su/library/pubs/aconf00/tconf00/ps/c6-4.pdf.

[14] R. C. Fernow, *Introduction to Experimental Particle Physics* (Cambridge University Press, New York, 2001).